Simultaneous liquid viscosity and density determination with piezoelectric unimorph cantilevers

Wan Y. Shih[a)]
Department of Materials Engineering, Drexel University, Philadelphia, Pennsylvania 19104-2875 and Department of Chemical Engineering and Princeton Materials Institute, Princeton University, Princeton, New Jersey 08544-5263

Xiaoping Li, Huiming Gu, and Wei-Heng Shih
Department of Materials Engineering, Drexel University, Philadelphia, Pennsylvania 19104-2875

Ilhan A. Aksay
Department of Chemical Engineering and Princeton Materials Institute, Princeton University, Princeton, New Jersey 08544-5263

(Received 4 January 2000; accepted for publication 31 May 2000)

We have examined both experimentally and theoretically a piezoelectric unimorph cantilever as a liquid viscosity-and-density sensor. The fabricated piezoelectric unimorph consisted of a $PbO \cdot ZrO_2 \cdot TiO_2$ (PZT) layer on a thin stainless-steel plate. In addition to a driving electrode, a sensing electrode was placed on top of the PZT layer, permitting the direct measurement of the resonance frequency. The cantilever was tested using water–glycerol solutions of different compositions. In all three of the tested modes, the resonance frequency decreased while the width of the resonance peak increased with increasing glycerol content. To account for the liquid effect, we consider the cantilever as a sphere of radius R oscillating in a liquid. By including the high and low frequency terms in the induced mass and the damping coefficient of the liquid, we show that for a given liquid density and viscosity the oscillating-sphere model predicts a resonance frequency and peak width that closely agree with experiment. Furthermore, the viscosity and the density of a liquid have been determined simultaneously using the experimentally measured resonance frequency and peak width as inputs to the oscillating-sphere model. The calculated liquid viscosity and density closely agreed with the known values, indicating that our cantilever-based sensor is effective in determining viscosity and density, simultaneously. We also show that scaling analysis predicts an increase in the width of the resonance peak with decreasing cantilever size, an observation in agreement with the large peak widths observed for microcantilevers. © *2001 American Institute of Physics.* [DOI: 10.1063/1.1287606]

INTRODUCTION

There has been a growing interest in *on-line* detection of liquid viscosity since it is a critical parameter sensitive to material property changes caused by chemical reaction, solidification, gelation, and/or deposition of substances.[1–6] *On-line* viscosity and density monitoring offers a powerful tool for monitoring the quality of a liquid and processes involving a liquid environment. For example, automobile engine oil undergoes both physical and chemical changes that degrade its performance over time. An *on-line* engine-oil viscosity sensor and indicator is of great interest to the automobile industry because it can remind the driver of the need for timely oil changes.[1] Similarly, in the colloidal processing of materials, uniformity in the suspension density is critical to the mechanical integrity of the final product.[7] Localized monitoring of viscosity and/or density presents a valuable means of controlling the spatial density variation in a suspension.

In recent years, a number of viscosity-sensing devices have been developed based on the mechanism of resonance, including $PbO \cdot ZrO_2 \cdot TiO_2$ (PZT)-disk oil viscosity sensors,[1] microfabricated-cantilever viscosity sensors,[2] quartz-membrane viscosity sensors,[3] and other types of ultrasonic viscosity sensors[4,5] including surface-acoustic-wave (SAW) viscosity sensors.[6] The idea behind all of these developments is the desire to detect a change in the resonance frequency and/or a change in the resonance peak width in the liquid, and from this deduce the liquid viscosity. Ultrasonic viscosity sensors are either based on thickness-mode resonance as in quartz-membrane viscosity sensors[3–5] or based on the resonance of the SAWs as in a Love-wave device.[4–6] The viscosity of a non-Newtonian liquid is known to be frequency (or rate) sensitive.[1,8] The operating frequency of ultrasonic viscosity sensors usually ranges from several MHz to a few hundred MHz. This is the frequency range where the viscosity of a non-Newtonian liquid can be substantially different from its low-frequency value that is often the quantity of interest.[1]

Furthermore, ultrasonic devices' high operating frequencies also limit the viscosity range over which they can be used.[6] Flexural modes generally have lower resonance fre-

a)Author to whom correspondence should be addressed; electronic mail: shihwy@drexel.edu

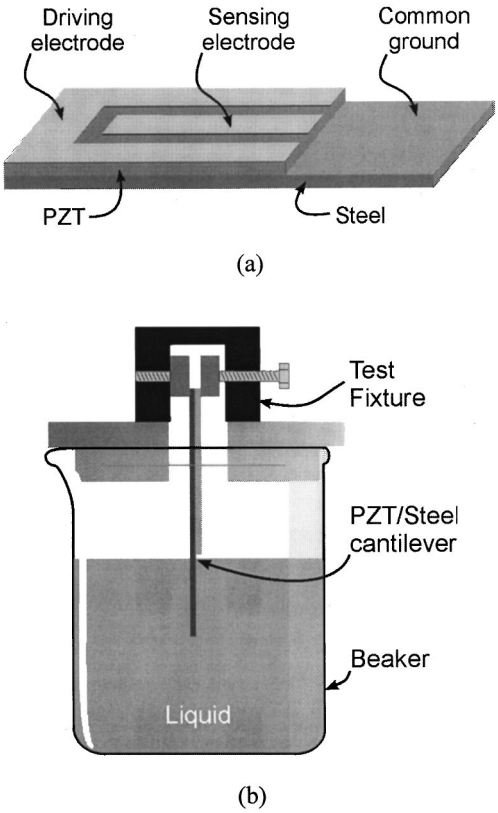

FIG. 1. A schematic of (a) the PZT/stainless-steel cantilever and (b) the setup of the viscosity sensing experiment.

quencies than the thickness modes or the radial modes. This makes flexural-mode devices better suited for sensing the low-frequency intrinsic viscosity of non-Newtonian liquids.[1] PZT-disk oil viscosity sensors[1] and the microcantilever viscosity sensors[2] both utilize flexural-mode resonance, allowing viscosity sensing at a lower frequency. The PZT-disk viscosity sensors demonstrated that the flexural mode could be used for engine oil viscosity sensing in the 30–150 cP range. However, the resonance-frequency change of the PZT-disk oil viscosity sensor is rather small ($<2.5\%$).[1] The microcantilevers have been used with a high sensitivity in the viscosity range of 1–200 cP. However, most of the work with microcantilever sensors has been through the use of an optical system to monitor the movement of the microcantilevers, which can limit their application in on-board or portable systems.

While the PZT-disk oil viscosity sensors and the microcantilevers demonstrated that they can be used for viscosity sensing it is not clear what controls the sensitivity and the viscosity range of a flexural-mode viscosity sensor. In this study, we examine the viscosity-and-density sensing capability of a flexural-mode device both experimentally and theoretically. Our flexural-mode viscosity-and-density sensor is a unimorph cantilever consisting of a piezoelectric, PZT layer and a stainless-steel layer (Fig. 1). The piezoelectricity of the PZT layer allows the resonance frequency to be detected directly with a dual-electrode design: one electrode for driving and one for sensing. That the resonance can be detected directly sets the piezoelectric cantilevers apart from silicon-based microcantilevers where vibrations must be detected with a laser beam or with a piezoresistive coating. On the theoretical side, we provide a fundamental understanding for the flexural-mode viscosity-and-density sensors through a detailed analysis and indicate how the sensitivity and viscosity range of flexural-mode sensors can be controlled. A scaling analysis is also provided to predict how the resonance frequency and the resonance peak width change with the size of the device.

TABLE I. Dimensions of PZT/steel cantilever.

	Length (cm)	Width (cm)	Thickness (mm)
PZT	3.05	0.6	0.56
Stainless steel	4.95	0.6	0.1

EXPERIMENTAL PROCEDURE

The PZT/steel unimorph cantilever was fabricated from an EC76 PZT thin sheet (EDO Corporation, Salt Lake City, UT) and a stainless steel foil (Shop-Aid Inc., Woburn, MA). A schematic of the cantilever is shown in Fig. 1(a). The silver-paste (Heraeus Inc., West Conshohocken, PA) driving and sensing electrodes were first painted on one side of the PZT, followed by heat treatment at 600 °C for 20 min. The U-shaped gray area along the rim of the PZT depicts the driving electrode. The long rectangular gray area along the central line of the cantilever is the sensing electrode. The sensing electrode allows the output signal to be detected directly with high sensitivity. After the driving and sensing electrodes were made, the other side of the PZT sheet was bonded to the stainless-steel foil using the same silver paste followed by the same curing procedure as in the top electrodes.

The dimensions of the PZT and the stainless steel sheets are listed in Table I. Note that the stainless-steel layer is longer than the PZT layer. The cantilever is clamped at the PZT end. The stainless-steel tip is the free end that is immersed in the liquid as illustrated in Fig. 1(b), serving as the sensing tip. The U-shaped outer electrode is connected to a functional generator to serve as the driving electrode. The rectangular inner electrode is connected to an oscilloscope to serve as the sensing electrode. When the driving frequency coincides with one of the resonance frequencies of the cantilever, a large voltage output can be obtained from the sensing electrode. The resonance spectra of the cantilever can also be obtained using an HP4192 impedance analyzer. In this case only the U-shaped outer electrode is connected to the impedance analyzer.

The solutions of glycerol and water of various glycerol concentrations were prepared as the test liquids. Specifically, water (0 wt % glycerol), a solution with 50 wt % glycerol and 50 wt % water (50 wt % glycerol), a solution with 75 wt % glycerol and 25 wt % water (75 wt % glycerol), and glycerol (100 wt % glycerol) were the four liquids used in this study. As shown in the schematic setup in Fig. 1(b), the PZT/steel cantilever was rigidly clamped at the PZT end with an aluminum fixture. The free stainless-steel end was immersed

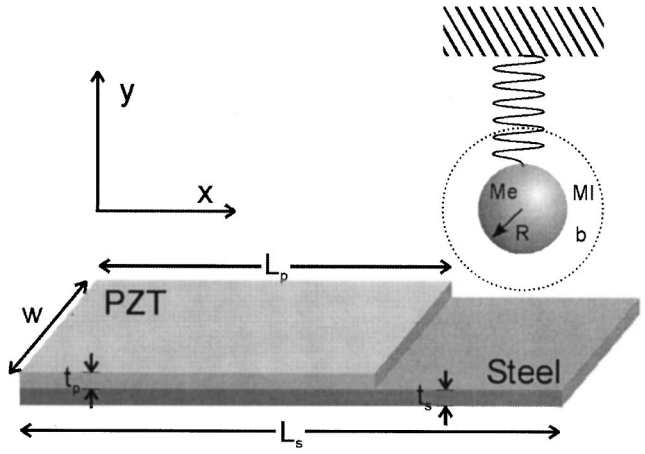

FIG. 2. A schematic of the cantilever.

in the test liquid. Two dipping depths were used: 1.5 and 0.76 cm. The viscosity of the glycerol–water solutions was also measured independently using a constant-stress rheometer (Rheometrics DSR).

THEORETICAL ANALYSIS

To consider the effect of the surrounding viscous liquid to an axially oscillating cantilever, we approximate the cantilever as an oscillating sphere immersed in a liquid as schematically illustrated in Fig. 2 following Ref. 2. The approximation is justified for: (i) the cantilever is much longer than it is wide, (ii) the axial displacement is significantly larger at and near the tip of a cantilever. In addition, the oscillating-sphere model allows an analytic expression for the drag force due to the liquid. As we will show below, the oscillating-sphere model works quite well for the present cantilever systems. When an oscillator is immersed in a liquid and driven by an external harmonic force $F_0e^{-i\omega t}$, the equation of motion for the oscillator in the axial direction y can be written as

$$(Me+MI)\frac{d^2y}{dt^2}+(b_{\text{in}}+b)\frac{dy}{dt}+Ky=F_0e^{-i\omega t}, \tag{1}$$

where ω is the angular frequency, Me and K the effective mass and effective spring constant at the tip of the cantilever respectively, MI and b the induced mass and the damping coefficient due to the viscous liquid, respectively, and b_{in} the intrinsic damping coefficient of the cantilever. The term $MI\,(d^2y/dt^2)$ represents the inertial force in potential flow past the cantilever and $b\,(dy/dt)$ the dissipative force due to the viscous drag. The intrinsic damping coefficient b_{in} may result in part from the glue between the PZT and the stainless steel and other internal dissipation mechanisms. For an oscillating sphere of an effective radius R in a liquid of density ρ and viscosity η both MI and b have analytic expressions[9]

$$MI=\frac{2\pi R^3}{3}\rho\left(1+\frac{9}{z}\frac{\delta}{R}\right), \tag{2}$$

and

$$b=\frac{6\pi\eta R^2}{\delta}\left(1+\frac{\delta}{R}\right), \tag{3}$$

where $\delta=\sqrt{2\eta/\rho\omega}$ is the decay length in the liquid. With low viscosity or high frequencies, δ is negligible compared to the effective radius R. The first term on the right-hand side of Eqs. (2) and (3) dominates and MI and b approach the high-frequency forms used in Ref. 2

$$MI_\infty=\frac{2\pi R^3}{3}\rho \tag{4}$$

and

$$b_\infty=\frac{6\pi\eta R^2}{\delta}, \tag{5}$$

where the subscript ∞ denotes $\omega\to\infty$. When the frequency approaches zero or the viscosity is high, the second term on the right hand side of Eqs. (2) and (3) dominates and MI and b approach

$$MI_0=3\pi R^2\,\delta\rho \tag{6}$$

and

$$b_0=6\pi\eta R, \tag{7}$$

where the subscript 0 denotes $\omega\to 0$. As we will show below, the low-frequency correction terms, i.e., Eqs. (6) and (7) [or the second term on the right-hand side of Eqs. (2) and (3)] become important when the liquid viscosity becomes high.

For a cantilever of density ρ, uniform thickness h, width w, and length L, the effective mass at the tip of the cantilever is $0.236\rho hwL$.[10] However, as shown in Fig. 1(a), the present cantilever has a thin stainless-steel overhang at the tip of the PZT/stainless steel section. Because the output electrical signal results from the piezoelectric effect in the PZT layer, what affects the output signal most is the vibration amplitude at the tip of the PZT layer. Therefore, we approximate the oscillating sphere to be located at the tip of the PZT layer (i.e., at $x=L_p$) but not at the tip of the stainless steel overhang (i.e., $x=L_s$), where L_p and L_s are, respectively, the length of the PZT layer and that of the stainless steel as illustrated in Fig. 2. The effective mass of the cantilever at the end of the PZT/stainless steel section (i.e., $x=L_p$) may be written as

$$Me=0.236(\rho_Ph_P+\rho_sh_s)wL_p+\rho_sh_sw(L_s-L_p), \tag{8}$$

where ρ_p, h_p, and L_p are the density, thickness, and length of the PZT layer, ρ_s and h_s the density and thickness of the stainless-steel layer, and w the width of the cantilever. The first term on the right hand side of Eq. (8) represents the effective mass of the PZT/stainless steel section at the tip of the PZT layer. The second term on the right hand side of Eq. (8) represents the effective mass of the stainless steel tip at the tip of the PZT layer. It is obtained by approximating the stainless-steel tip to be an attachment at the tip of the PZT layer that moves at the same velocity as the tip of the PZT layer (or the PZT/stainless-steel section). The approximation was justified for: (i) the stainless steel tip is much lighter than the PZT/stainless steel section and (ii) no PZT layer is

on top of the stainless steel tip to actuate it. Because the stainless steel tip is much thinner than the PZT/stainless-steel section and the bending modulus is a third-power function of the thickness, it is justifiable to neglect the stainless-steel tip in estimating the effective spring constant at the tip of the PZT/stainless-steel section.

Neglecting the stainless-steel tip, the effective spring constant K at the tip of the PZT/stainless steel section may be approximated as[10]

$$K=\frac{3D_P w}{L_p^3}, \tag{9}$$

where D_P is the bending modulus of the PZT/stainless steel section which can be written as[11]

$$D_P=w\frac{E_p^2h_p^4+E_s^2h_s^4+2E_pE_sh_ph_s(2h_p^2+2h_s^2+3h_ph_s)}{12(E_ph_p+E_sh_s)}, \tag{10}$$

where E_p and E_s are the Young's modulus of the PZT layer and that of the stainless-steel layer, respectively.

The lowest resonance frequency in air can be approximately expressed in terms of K and Me as[10]

$$f_1=\frac{1}{2\pi}\sqrt{\frac{K}{Me}}. \tag{11}$$

For higher-mode resonance, the resonance frequency may also be expressed in terms of K and Me as

$$f_i=\frac{n_i}{2\pi}\sqrt{\frac{K}{Me}}, \tag{12}$$

where n_i is the ith-mode eigenvalue.

When the cantilever is immersed in a liquid, with $y=y_0e^{-i\omega t}$, Eq. (1) gives the axial amplitude y_0 as

$$y_0=\frac{-F_0}{(\omega^2-\omega_0^2)+i\omega\gamma}, \tag{13}$$

and the maximum in $|y_0|$ occurs at $\omega=\omega_{\max}$ where

$$\omega_{\max}^2=\omega_0^2-\tfrac{1}{2}\gamma^2, \tag{14}$$

with

$$\omega_0=\sqrt{\frac{K}{Me+MI}} \tag{15}$$

being the resonance frequency without damping and

$$\gamma=\frac{b+b_{\text{in}}}{Me+MI} \tag{16}$$

being the damping coefficient per unit mass. Note that at $\omega=\omega_{\max}$, both $|y_0|$ and $\mathrm{Im}(y_0)$ have a peak value $F_0/\omega_{\max}\gamma$. However, the peak widths at half the peak height are $\sqrt{3}\gamma$ and γ for $|y_0|$ and $\mathrm{Im}(y_0)$, respectively. Thus, as γ increases, the resonance peak width increases. Furthermore, as can be seen from Eqs. (14)–(16), both the increase in the liquid induced mass and that in the liquid damping coefficient can lower the resonance frequency.

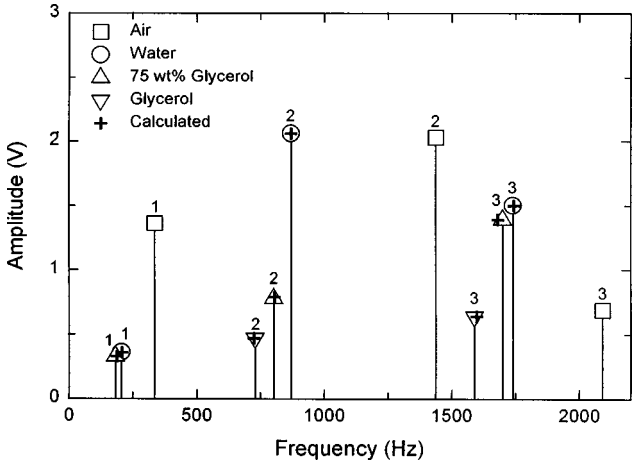

FIG. 3. Resonance frequency spectrum of the cantilever in air (open squares), water (open circles), 75 wt % glycerol (open up triangles), and glycerol (open down triangles) obtained using the sensing electrode. The vertical axis indicates the voltage difference obtained at the sensing electrode with a 10 V driving voltage applied at the driving electrode. The dipping depth is 1.5 cm for all liquids. The crosses indicate the calculated resonance frequencies under various liquid environments.

RESULTS AND DISCUSSIONS

Figure 3 summarizes the cantilever's resonance-frequency spectra obtained from the sensing electrode for frequencies below 2500 Hz. In this frequency range, the cantilever exhibits three in-air resonance frequencies (open squares): 334 Hz (mode 1), 1432 Hz (mode 2), and 2090 Hz (mode 3). Using Eqs. (8)–(11) and the parameters listed in Table I, the calculated value for f_1 is 330 Hz, in agreement with the lowest measured resonance frequency in air, 334 Hz, as shown in Fig. 3. The agreement between the experimental and estimated lowest resonance frequency in air indicates that the approximated effective mass Me and the effective spring constant K for the cantilever are reasonable. Meanwhile, using Eq. (12), the eigenvalues for mode 2 and mode 3 resonance can be deduced empirically. We obtained $n_i=4.3$ and 6.25 for mode 2 and mode 3, respectively. For a cantilever with a uniform cross section, the second mode eigenvalue is 6.25.[10] This indicates that the mode 2 resonance obtained with the present cantilever would not appear if the cantilever had constant thickness throughout the length.

Also shown in Fig. 3 are the resonance-frequency spectra with a 1.5 cm dipping depth in water (open circles), in 75 wt % glycerol (open up triangles), and in glycerol (open down triangles). In water, the resonance frequencies of mode 1, mode 2, and mode 3, respectively, decreased to 212, 870, and 1730 Hz. In 75 wt % glycerol, the three resonance frequencies were further decreased from 334, 1432, and 2090 Hz to 190 (mode 1), 805 (mode 2), 1700 Hz (mode 3). In glycerol, the lowest resonance frequency (mode 1) was not observable. The two higher resonance frequencies were observed at 733 (mode 2) and 1630 Hz (mode 3). It is clear that in all three modes, the resonance frequency decreases as the glycerol content of the liquid increases. As we will show below, the shift in the resonance frequency is closely related to the change in the viscosity as well as in the density of the

TABLE II. Density and viscosity of water–glycerol mixtures. The viscosity listed below was obtained from the rheological measurement.

	Density (kg/m^3)	Viscosity (P)
Water	1000	0.01
50 wt % glycerol	1100	0.04
75 wt % glycerol	1180	0.4
Glycerol	1260	6

test liquid. As listed in Table II, both the viscosity and the density of the test liquid increase with the glycerol content. Besides the shift in the resonance frequency, a more viscous liquid also makes the resonance peak broader as we discussed in the previous section. As an example, Fig. 4 shows the phase-angle spectra obtained from the impedance analyzer at the second resonance (mode 2) of the cantilever in various water/glycerol solutions with a 1.5 cm dipping depth. Clearly, as the viscosity of the liquid increases with the glycerol content, the height of the resonance peak progressively decreases and the peak width increases. The peak widths at half peak height $\gamma/2\pi$ determined from Fig. 4 are listed in Table III.

To examine the sensitivity of the three resonance modes in terms of resonance frequency change by the surrounding liquid, we use $\Delta f/f_w=(f_w-f_{75\%})/f_w$ as a measure, where f_w and $f_{75\%}$ are, respectively, the resonance frequency in water and that in 75 wt % glycerol. The obtained $\Delta f/f_w$ for the three modes are listed in Table IV. It can be seen that among the three modes, mode 1 has the highest sensitivity, with $\Delta f/f_w \cong 11\%$. Moreover, a different dipping depth also affects the resonance-frequency change and the peak width. For example, listed in Table V are the mode 2 resonance frequencies and peak widths in various liquid environments with a 0.75 dipping depth. The resultant $\Delta f/f_w$ for the mode 2 resonance with a 0.75 cm dipping depth in various liquid environments is also listed in Table V. Compared to a 1.5 cm dipping depth, the 0.75 dipping depth gives a smaller change in the resonance frequency. The $\Delta f/f_w$ decreases from about 7.7% at a 1.5 cm dipping depth to about 4% at a 0.75 cm dipping depth.

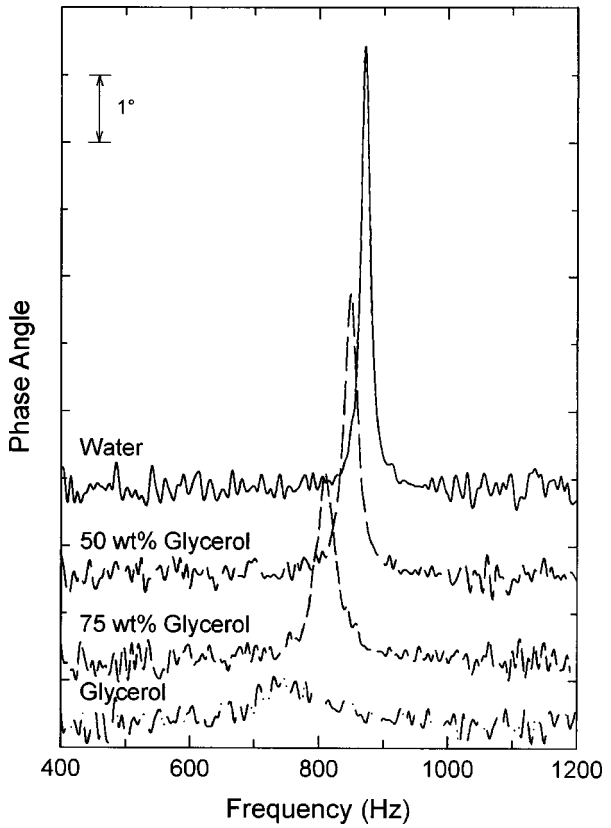

FIG. 4. Phase angle vs frequency of the PZT/steel cantilever with a 1.5 cm dipping depth in water, 50 wt % glycerol, 75 wt % glycerol, and glycerol around the mode 2 resonance frequency. Different curves are vertically shifted for clarity.

TABLE III. Mode 2 resonance frequency f_{max} and peak width $\gamma/2\pi$ with a 1.5 cm dipping depth. The experimental values of $\gamma/2\pi$ were determined from the phase angle data shown in Fig. 4. The calculated values of $\gamma_{liq}/2\pi$ and those of $\gamma/2\pi$ are obtained using $\gamma_{liq}/2\pi=(1/2\pi)/[b/(Me+MI)]$ and $\gamma/2\pi=(1/2\pi)/[(b+b_{in})/(Me+MI)]$, respectively, where Me is the effective mass of the cantilever, MI the induced mass from the liquid, b the damping coefficient from the liquid, and b_{in} the intrinsic damping coefficient of the cantilever.

	f_{max} cal. (Hz)	f_{max} exp. (Hz)	$\gamma/2\pi$ exp. (Hz)	$\gamma/2\pi$ cal. (Hz)	$\gamma_{liq}/2\pi$ cal. (Hz)
Water	870	870	19	18	7
50 wt % glycerol	840	844	28	25	14
75 wt % glycerol	805	803	42 ± 10	51	42
Glycerol	725	733	140 ± 20	145	138

With a piezoelectric unimorph cantilever, the axial displacement can be detected from the sensing electrode as an induced voltage difference across the thickness. From the direct voltage measurement as a function of frequency in Hz, both the resonance frequency $f_{max}=\omega_{max}/2\pi$ and the damping factor per unit mass $\gamma/2\pi$ can be obtained.

Alternatively, the axial displacement can be detected from the impedance measurement as well. For convenience, all peak widths reported from this work were obtained from the impedance analyzer. Far away from the resonance frequency, the unimorph cantilever behaves as a capacitor. Therefore, the impedance of the unimorph can be generally expressed as

$$z=\frac{-i}{\omega c}+iz_i, \tag{17}$$

where c is the capacitance of the unimorph, and iz_i the induced impedance due to the flexural displacement. This can

TABLE IV. $\Delta f/f_w$ and R in various resonance modes where $\Delta f/f_w$ measures the sensitivity and R is the radius of the effective sphere.

	1.5 cm dipping depth		0.75 cm dipping depth	
Mode	$\Delta f/f_w$	R (mm)	$\Delta f/f_w$	R (mm)
1	11%	7.80	⋯	⋯
2	7.7%	6.31	4%	3.55
3	2.3%	5.05	⋯	⋯

TABLE V. Mode 2 resonance frequency f_{max} and peak width $\gamma/2\pi$ with a 0.75 cm dipping depth. The experimental values were determined from the phase angle data (not shown).

	f_{max} cal. (Hz)	f_{max} exp. (Hz)	$\gamma/2\pi$ exp. (Hz)	$\gamma/2\pi$ cal. (Hz)	$\gamma_{liq}/2\pi$ cal. (Hz)
Water	1257	1260	24	26	6
50 wt % glycerol	1238	1232	35	32	12
75 wt % glycerol	1214	1209	48 ± 10	58	38
Glycerol	1147	1140	140 ± 20	160	142

be seen by plotting the impedance $|z|$ versus f on a log–log scale where $\log|z|$ is linear in $\log f$ with a slope of -1 (see Fig. 5 where the impedance $|z|$ is plotted versus f for a 1.5 dipping depth in water, 50 wt % glycerol, 75 wt % glycerol, and glycerol). For the present cantilever, the deduced capacitance is $c=6.0$ nF. The induced impedance iz_i is related to the axial displacement and can be expressed as

$$iz_i=\frac{i\alpha}{(\omega^2-\omega_0^2)+i\omega\gamma}, \tag{18}$$

where α is a proportional constant. Note that in electrical measurements, the real part of z, $\mathrm{Re}(z)$, relates to dissipation, whereas in the displacement measurement it is the imaginary part of y_0, $\mathrm{Im}(y_0)$, which is related to dissipation. Therefore, $\mathrm{Re}(z)$ is proportional to $\mathrm{Im}(y_0)$. Knowing that $\mathrm{Re}(z)$ is proportional to $\mathrm{Im}(y_0)$, we can also obtain f_{max} and $\gamma/2\pi$ from the peak position and peak width at half the peak height of $\mathrm{Re}(z_i)$ versus f. In the present system, the background term $-i/\omega c$ is the dominant term as can be seen from Fig. 5. The phase angle θ is always close to $-90°$ (see Fig. 4). Therefore, $\mathrm{Re}(z)$ is roughly linear with $\Delta\theta\equiv\theta+90$. Thus, f_{max} and $\gamma/2\pi$ can be obtained from the peak position and the peak width at half the peak height of $\Delta\theta$ versus f (or θ versus f as shown in Fig. 4) as well. The f_{max} and $\gamma/2\pi$ obtained from $\mathrm{Re}(z_i)$ versus f (not shown) are essentially the same as those deduced from θ versus f. In the following, all the values of f_{max} and $\gamma/2\pi$ were obtained from the θ versus f plots.

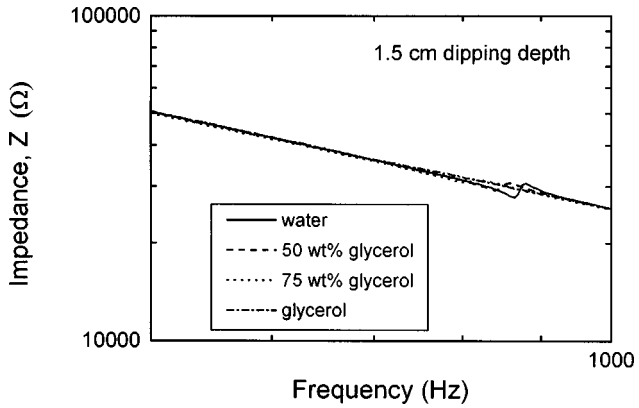

FIG. 5. $|z|$ vs f in a log–log plot near the mode 2 resonance frequency in water, 50 wt % glycerol, 75 wt % glycerol, and glycerol with a 1.5 cm dipping depth where $|z|$ is the absolute value of the impedance and f the frequency. The $\log(|z|)$ is linear in $\log(f)$ with a slope -1 indicates that the cantilever is mainly a capacitor with a capacitance of 6.0 nF.

With known ρ and η, we can solve Eqs. (15) and (16) to obtain the resonance frequency f_{max} and the peak width $\gamma/2\pi$, provided the effective radius R and the intrinsic damping coefficient of the cantilever b_{in} are known. Conversely, with the measured f_{max} and $\gamma/2\pi$, we can also solve Eqs. (15) and (16) for the liquid density ρ and the liquid viscosity η. It is this latter approach that allows the cantilever to be a viscosity-and-density sensor.

With the known effective mass of the cantilever Me, one can obtain the intrinsic damping coefficient b_{in} from the resonance peak in air. We obtained $b_{in}/2\pi\cong9.0\times10^{-3}$ Hz/kg. To obtain R empirically, we fit the resonance frequency f_{max} in water to the measured value using the known density and viscosity of water. For a dipping depth of 1.5 cm, we obtain $R=7.8$, 6.315, and 5.05 mm for mode 1, mode 2, and mode 3 resonance, respectively, which are listed in Table IV along with $\Delta f/f_w$. From Table IV, it is clear that for a given dipping depth, $\Delta f/f_w$ increases with R. Mode 1, which has the largest R, shows the highest $\Delta f/f_w$. This may be qualitatively understood as follows. In a Mode 1 vibration, the entire cantilever moves in the same direction as the tip, whereas at higher modes the number of nodes increases with an increasing resonance frequency. Thus at higher modes only an increasingly smaller part of the cantilever moves in the same direction as the tip, resulting in a smaller R. Meanwhile, for the same resonance mode, a smaller dipping depth can also give a smaller R. For example, R for the mode 2 vibrations reduced from 6.315 to 3.55 mm when the dipping changed from 1.5 to 0.75 cm. As $\Delta f/f_w$ decreases with a decreasing R, this in turn reduces $\Delta f/f_w$ from 7.7% to 4% when the dipping depth changes from 1.5 to 0.75 cm.

Knowing the effective radius R, the liquid density, and the liquid viscosity, the corresponding resonance frequency in the liquid can be obtained by solving Eqs. (15) and (16) using Eqs. (2) and (3) to calculate MI and b. The obtained resonance frequency is also plotted in Fig. 3 to compare with the experimental results. It is clear that the calculated resonance frequencies are in close agreement with the experimental result. To see how the liquid viscosity and density affect the resonance-frequency shift, we calculate f_0 using MI_∞ and b_∞ as depicted in Eqs. (4) and (5) instead of the MI and b depicted in Eqs. (2) and (3). The quantity f_0, represents the high-frequency-limit resonance frequency of the cantilever surrounded by a liquid. The obtained values of f_0 along with f_{max} are plotted in Fig. 6 as a function of η with both 1.5 and 0.75 cm dipping depths. Also plotted in Fig. 6 are the experimental resonance frequencies. Here, f_{max} agrees with the experimental resonance frequencies better than f_0, especially when the viscosity becomes higher than or equal to 40 cP. The reason that f_0 does not agree with the experimental resonance frequency as well as f_{max} when the viscosity becomes high is that Eqs. (4) and (5) do not represent the induced mass and the damping coefficient correctly because δ/R is not negligibly small at higher viscosity. For example, in glycerol, $\delta/R\cong0.085$. Thus, when Eq. (4) is used instead of Eq. (2), the MI for glycerol is underestimated by about 18%, which in turn leads to an overestimation of the resonance frequencies as can be seen from Fig. 6. Similar overestimation of the resonance frequency by using the high-

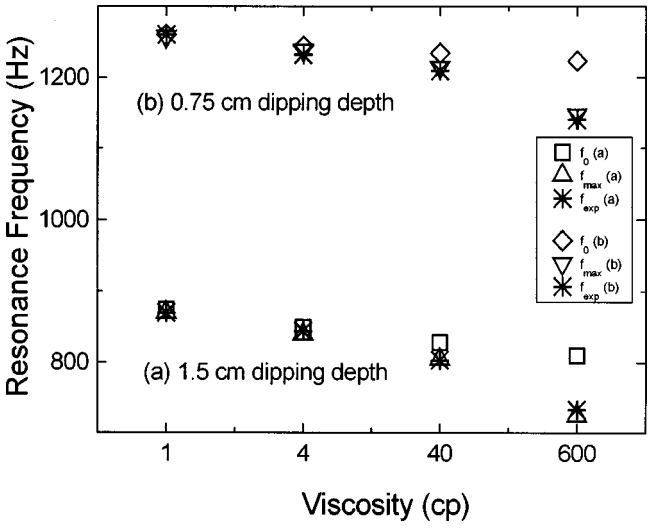

FIG. 6. f_{max} and f_0 vs η, where η is the viscosity and f_{max} and f_0 are the calculated resonance frequencies with and without the high-viscosity terms [Eqs. (11) and (12)] for the induced mass and the damping coefficient (a) for a 1.5 cm dipping depth and (b) for the 0.75 cm dipping depth. Also plotted are the experimental resonance frequencies where for all cases, f_{max} agrees better with the experimental resonance frequencies indicating that the high-viscosity terms are important.

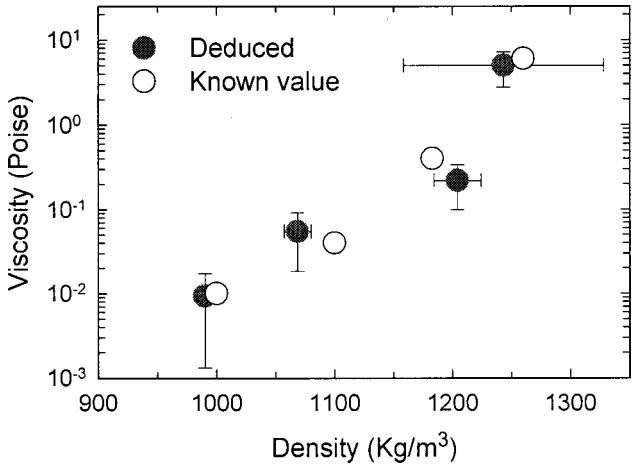

FIG. 7. Deduced density ρ and viscosity η (open circles) of the four liquids examined plotted on the two-dimensional η–ρ plane. Also plotted are the known values (full circles) of ρ and η of the four liquids. The deduced ρ and η were obtained with the mode 2 resonance frequencies and peak widths with a 1.5 cm dipping depth.

frequency expressions for MI and b is also apparent in Ref. 2 where only the high-frequency terms, Eqs. (4) and (5), were considered for MI and b. From Fig. 6, it is clear that at higher viscosity, Eqs. (2) and (3) should be used for MI and b so that the resonance-frequency shift can be calculated correctly. The calculated values for $\gamma_{liq}/2\pi=(1/2\pi)(b/Me+MI)$ are also listed in Table II. With $b_{in}/2\pi=9.0\times10^{-3}$ Hzkg, the calculated values for $\gamma/2\pi=(1/2\pi)(b+b_{in})/(Me+MI)$ in various liquid environments are also listed in Table II. It can be seen that the calculated values for $\gamma/2\pi$ are also in close agreement with the measured results.

Conversely, the liquid viscosity η and liquid density ρ can be determined simultaneously by solving Eqs. (15) and (16) using the measured f_{max} and $\gamma/2\pi$ as the input and MI and b calculated using Eqs. (2) and (3). For example, the resultant ρ and η of the tested liquids are plotted in Fig. 7 using f_{max} and $\gamma/2\pi$ from the mode 2 oscillations with a 1.5 dipping depth. The known values of ρ and η are also plotted in Fig. 7. For all four tested liquids, the deduced ρ and η are in good agreement with the known values of ρ and η of the tested liquids This demonstrates that with the present approach, the cantilever can indeed be used as a simultaneous viscosity-and-density sensor.

SIZE EFFECT: SCALING ANALYSIS

Presently, there is tremendous interest in miniaturizing the cantilevers as microsensors[2,12–14] for medical and other purposes. It is important to understand how the change in the dimension of the cantilever affects the damping coefficient and therefore the sensitivity of the cantilever in a liquid environment. To examine the effect of miniaturization, let us first look at the induced mass as listed in Table II and compare it with the cantilever's own effective mass. With 1.5 cm dipping depth, $MI=1.0\times10^{-3}$ and 1.97×10^{-3} kg, for a mode 1 resonance in water and that in 75 wt% glycerol, respectively. Both values are much larger than the cantilever's own effective mass $Me=3.09\times10^{-4}$ kg. Therefore, in the following scaling analysis, we will neglect Me and consider only the induced mass MI. Let us consider a cantilever that shrinks in all three dimensions by a factor β as schematically shown in Fig. 8. As a result, the effective spring

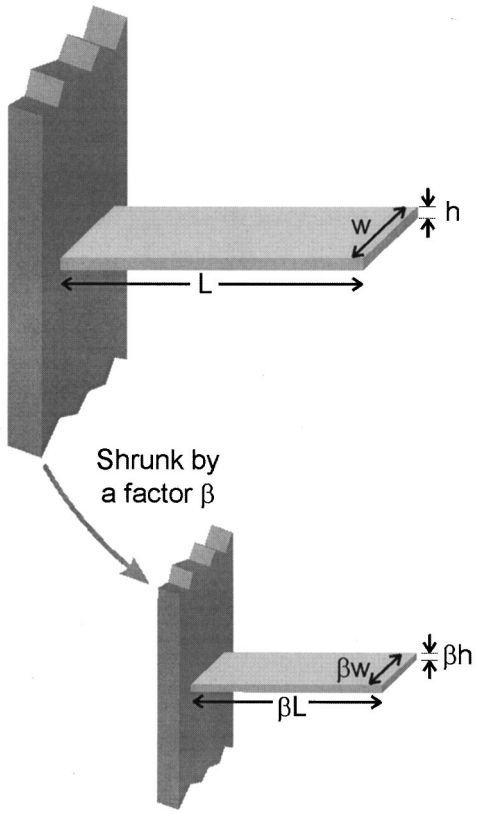

FIG. 8. A schematic showing: (a) a cantilever of length L, width w, and thickness h, and (b) the cantilever with all dimensions reduced in proportion by a factor β, i.e., length βL, width βw, and thickness βh.

constant $k(\beta)$ of the shrunk cantilever scales as

$$K(\beta) \propto \beta K, \tag{19}$$

where K is the spring constant of the cantilever before shrinking. We will separate the discussions into two regimes, i.e., the high frequency regime and the low frequency regime.

(i) High-frequency or low viscosity regime. In the high frequency regime, the induced mass [Eq. (4)] for the shrunk cantilever is

$$MI_{\infty}(\beta) \propto \beta^3. \tag{20}$$

Therefore,

$$f_i(\beta) \approx \sqrt{\frac{K(\beta)}{MI_{\infty}(\beta)}} \propto \beta^{-1}. \tag{21}$$

In this regime, the resonance frequency increases as the size of the cantilever decreases. The damping factor $b_{\infty}(\beta)$ as depicted in Eq. (5) and the damping factor per unit mass $\gamma_{\mathrm{liq}}(\beta)$ of the shrunk cantilever, respectively, are

$$b_{\infty}(\beta) \propto \beta^2 (f(\beta))^{1/2} \propto \beta^{3/2}, \tag{22}$$

and

$$\gamma_{\mathrm{liq}}(\beta) = \frac{b_{\infty}(\beta)}{MI_{\infty}(\beta)} \propto \beta^{-3/2}. \tag{23}$$

As $\gamma_{\mathrm{liq}}(\beta)$ determines the width at half the peak height, one expects that as the cantilever shrinks the resonance peak becomes broader according to Eq. (23). The quality factor defined as $Q = f_{\max}/\gamma$ also becomes smaller as

$$Q(\beta) \propto \beta^{1/2} Q. \tag{24}$$

(ii) Low-frequency or high-viscosity regime. In this regime, the induced mass [Eq. (6)] for the shrunk cantilever becomes

$$MI_0(\beta) \propto \beta^2 f_i^{-1/2}, \tag{25}$$

where f_i is the resonance frequency without damping

$$f_i(\beta) \propto \sqrt{\frac{K(\beta)}{MI_0(\beta)}}. \tag{26}$$

Combining Eqs. (25) and (26), we get

$$MI_0(\beta) \propto \beta^{7/3}, \tag{27}$$

and

$$f_i(\beta) \propto \beta^{-2/3}. \tag{28}$$

The damping factor, $b_0(\beta)$ [Eq. (7)] and the damping factor per unit mass $\gamma_{\mathrm{liq}}(\beta)$ of the shrunk cantilever, respectively, are

$$b_0(\beta) \propto \beta^1, \tag{29}$$

and

$$\gamma_{\mathrm{liq}}(\beta) = \frac{b_0(\beta)}{MI_0(\beta)} = \beta^{-4/3}. \tag{30}$$

Therefore, in the low-frequency, high-viscosity regime, $\gamma_{\mathrm{liq}}(\beta)$ increases as $\beta^{-4/3}$, slower than in the high-frequency, low viscosity regime. The quality factor decreases as

$$Q(\beta) = \frac{f_i(\beta)}{\gamma_{\mathrm{liq}}(\beta)} \propto \beta^{2/3}, \tag{31}$$

faster than in the high-frequency, low-viscosity regime.

In the experiments, the condition is somewhere inbetween the two regimes. One expects that the scaling of γ_{liq} and Q with respect to β will be between Eqs. (23) and (24), and Eqs. (30) and (31). From the above scaling analysis, one can see that the resonance peak of a cantilever in a liquid will become broader as the dimension of the cantilever is reduced. Moreover, the broadening of the resonance peak with respect to a decreasing cantilever size is more pronounced in the low-frequency, high-viscosity regime than in the high-frequency, low-viscosity regime. The broadening effect will no doubt increase the sensitivity of the viscosity measurement. Meanwhile, the resonance frequency increases with decreasing cantilever size in both regimes although the increase in the resonance frequency with decreasing cantilever size is not as steep in the low-frequency or high-viscosity regime. This difference will also enhance the sensitivity of the resonance frequency change with respect to viscosity when a smaller cantilever is used.

Although the geometry of the present cantilever is not exactly in proportion to the microcantilevers used in Ref. 2, we can still compare the results of the present study with that in Ref. 2 to see how the sensitivity of the measurements changes as the dimension of the cantilever shrinks. The present cantilever that is about 3 cm long is about two orders of magnitude longer than the microcantilevers used in Ref. 2 which are about 100 μm long. In water, the lowest resonance frequency in the present system is about 212 Hz. The microcantilevers' resonance frequencies in water were about 25 kHz, about two orders of magnitude higher than that of the present study, in line with the scaling result shown in Eq. (21) which predicts that the resonance frequency is inversely proportional to the dimension of the cantilever. When immersed in a more viscous liquid, for example, the present cantilever has a resonance frequency of about 190 Hz in 75 wt % glycerol. The microcantilevers' resonance frequencies in 90% glycerol were about 5 kHz, about 25 times higher than the resonance frequency of the present cantilever. This also supports the scaling result that the resonance frequency increases less steeply with a decreasing cantilever size in the high-viscosity regime than in the low-viscosity regime [see Eqs. (21) and (28)]. For peak broadening, in the present experiment, $\gamma/2\pi$ is about 20 Hz in water. In comparison, the microcantilevers had a $\gamma/2\pi$ on the order of kHz in water, about two orders of magnitude higher than that of the present cantilever, also qualitatively in line with prediction of Eqs. (23). In a more viscous liquid, the present cantilever has a $\gamma/2\pi$ about 140 Hz. The microcantilevers had a $\gamma/2\pi$ about 2 kHz, about one order of magnitude higher than that of the present study, also qualitatively in line with the prediction that γ_{liq} increases less rapidly with a reduced cantilever size

in the high-viscosity regime than in the low-viscosity regime [see Eqs. (23) and (30)].

CONCLUSIONS

We have examined both experimentally and theoretically a piezoelectric unimorph cantilever as a liquid viscosity-and-density sensor. The piezoelectric unimorph consists of a PZT layer on top of a thin stainless-steel layer. In addition to a driving electrode, a sensing electrode is also fabricated on the top surface of PZT, allowing the resonance frequency to be detected simply, enabling the cantilever to be easily integrated in on-board or portable applications. Water–glycerol solutions of various glycerol concentrations were used as the test liquids. In all three modes examined in the frequency range <2500 Hz, the resonance frequency decreases while the width of the resonance peak increases with an increasing glycerol content. We consider the effect of the liquid on the cantilever by modeling the cantilever as an oscillating sphere with an effective radius R. By including both the high-frequency, low-viscosity term [Eqs. (4) and (5)] and the low-frequency, high-viscosity term [Eqs. (6) and (7)] in Eqs. (2) and (3) for the induced mass and the damping coefficient of the liquid, we showed that the oscillating-sphere model predicts resonance frequencies and peak widths that are in close agreement with the experimental data for viscosity ranging from 1 to 600 cP. The consideration of the high-viscosity term, i.e., Eqs. (6) and (7), are crucial for obtaining the right resonance frequencies and right peak width in the high viscosity regime.

The effective radius of the oscillating sphere R varies with both the dipping depth and the in-air resonance frequency. For a given depth, the effective R increases with a decreasing in-air resonance frequency. The sensitivity $\Delta f/f_w$ increases with a decreasing in-air resonance frequency (due to an increasing R where f_w is the resonance frequency in water and $\Delta f=f_{75}-f_w$ with f_{75} being the resonance frequency in 75 wt% glycerol. Within a given mode, a larger dipping depth also increases R and hence the sensitivity.

To demonstrate the cantilever's capability for sensing the liquid viscosity and the liquid density simultaneously, we us the experimental mode 2 $f_{\max}$ and $\gamma/2\pi$ with 1.5 cm dipping depth as the input and solved Eqs. (15) and (16) for the liquid viscosity and the liquid density simultaneously using the oscillating-sphere model [Eqs. (2) and (3)]. The deduced liquid viscosity and liquid density are in close agreement with the known values, indicating that the cantilever in the present approach can be an effective viscosity-and-density sensor.

A scaling analysis is also included to predict how the resonance frequency as well as the sensitivity of the measurement varies as the size of the cantilever is reduced. It is predicted that both the resonance frequency and the width of the resonance peak increase with a decreasing size in both the low-viscosity regime [Eqs. (21) and (23)] and the high-viscosity regime [Eqs. (28) and (30)]. The higher resonance frequencies and peak widths obtained from the microcantilevers qualitatively support these scaling analyses.

ACKNOWLEDGMENT

This work was supported by the Army Research Office Multidisciplinary University Research Initiative (MURI) under Grant No. DAAH04-95-1-0102.

[1] J. Sorab, G. S. Saloka, and A. H. Meitzler, SAE Technical Paper No. 971704 (May 1997).
[2] P. I. Oden, G. Y. Chen, R. A. Steele, R. J. Warmack, and T. Thundat, Appl. Phys. Lett. **68**, 3814 (1996).
[3] Z. Lin, C. M. Yip, I. S. Joseph, and M. D. Ward, Anal. Chem. **65**, 1546 (1993).
[4] P. Hauptmann, R. Lucklum, A. Püttmer, and B. Henning, Sens. Actuators A **67**, 32 (1998).
[5] D. S. Ballantine, R. M. White, S. J. Martin, A. J. Ricco, E. T. Zellers, G. C. Frye, and H. Wohltjen, *Acoustic Wave Sensors* (Academic, San Diego, CA, 1997).
[6] B. Jakoby and M. J. Vellekoop, Sens. Actuators A **68**, 275 (1998).
[7] V. K. Pujari, D. M. Tracey, M. R. Foley, N. I. Paille, P. J. Pelletier, L. C. Sales, C. A. Willkens, and R. L. Yeckley, Am. Ceram. Soc. Bull. **74**, 86 (1995).
[8] J. D. Ferry, *Viscoelastic Properties of Polymers* (Wiley, New York, 1980).
[9] L. D. Landau and E. M. Lifshitz, *Fluid Mechanics* (Pergamon, London, 1959), p. 96.
[10] J. Merhaut, *Theory of Electroacoustics* (McGraw–Hill, New York, 1981), p. 100.
[11] X. Li, W. Y. Shih, I. A. Aksay, and W.-H. Shih, J. Am. Ceram. Soc. **82**, 1733 (1999).
[12] A. N. Cleland and M. L. Roukes, Appl. Phys. Lett. **69**, 2653 (1996).
[13] S. R. Manalis, S. C. Minne, and C. F. Quate, Appl. Rev. Lett. **70**, 3311 (1997).
[14] D. L. Polla and L. F. Fracis, Annu. Rev. Mater. Sci. **28**, 563 (1998).